ORIGINAL PAPER

Hydrodynamic-sediment transport response to waterway depth in the Three Gorges Reservoir, China

Yi Xiao[1] · Wenjie Li[1] · Shengfa Yang[1]

Abstract

Since the Three Gorges Dam began operation in 2003, hydrodynamic-sediment conditions changes have occurred not only downstream but also in the Three Gorges Reservoir, contributing to variations in the navigation conditions of the backwater area. Based on the measured channel data from 2003 to 2018, this study investigates changes in the waterway dimension and the factors that impact navigation conditions. The navigation-obstructing channels in the permanent backwater area (PBA) mainly resulted from the occurrence of fine grained sedimentation, which led to a decrease in the effective navigable width. Meanwhile, in the fluctuating backwater area (FBA), bed load behavior during the falling stage from April to June lowered navigation depths. Decreasing sediment supply can alleviate reservoir sedimentation and maintain navigation safety in the PBA, while it is necessary to focus on the waterway depth clearance that is sensitive to temporary deposition during the falling stage of high water-sediment discharge years in the FBA. Water level variation near gravel excavation pits indicates that sediment mining decreases waterway depth, negatively impacting the navigable dimension, especially during low water discharge. These findings provide useful information for assessing the sustainable development of the navigation in the Three Gorges Reservoir, and aid economic development in the Yangtze River.

Keywords Navigation condition · Water-sediment discharge · Sedimentation · Bed load behavior · Three Gorges Reservoir · 2D numerical model

Introduction

Over the past century, many of the world's major rivers have been modified for the purposes of flood mitigation, power generation, and commercial navigation (Munoz et al. 2018). The Yangtze River is Asia's longest (6300 km) river and the fifth largest in the world (Milliman and Meade 1983). The upper Yangtze River comprises alluvial gravel, riffle, and pool channel form, wherein its bed passes through geologically old gravel deposits (Chen et al. 2001). The river flows through the subtropical region with a mean temperature and precipitation of 20 °C and 870 mm, respectively (Wang et al. 2007). The Three Gorges Dam (TGD) on the upper Yangtze River is a

key project for the river's flood control, navigation, and water resource development (Jia et al. 2013). After the impoundment of the TGD, the normal pool level was 175 m with a water storage capacity of 39.3 billion m^3, and a flood control level of 145 m with a flood control capacity of 22.15 billion m^3 (Zheng 2016). The TGD holds a reservoir that is 660 km long, stretching from Yichang to Jiangjin Town in Chongqing, and is divided into permanent and fluctuating backwater areas at the Fuling station (Fig. 1).

The operation of the TGD has led to sedimentation in the backwater area (60% of that predicted in the planning stage), and widespread scouring in the reaches below the dam was caused by a rapid decrease in the downstream sediment load (CWRC 2019). Regarding the TGD downstream, several studies have documented the spatial and temporal changes of water-sediment discharge (Xu and Milliman 2009; Xiong et al. 2009; Dai and Lu 2014; Mei et al. 2015; Li et al. 2018a; Xiao et al. 2019a; Ren et al. 2020), channel adjustment processes (Li et al. 2009; Sun et al. 2012; Dai and Liu 2013; Zhou et al. 2017), material fluxes and water exchanges between the downstream and large lakes (Yuan et al. 2015; Huang et al.

Responsible Editor: Broder J. Merkel

✉ Yi Xiao
xymttlove@163.com

[1] National Inland Waterway Regulation Engineering Research Center, Chongqing Jiaotong University, Chongqing, China
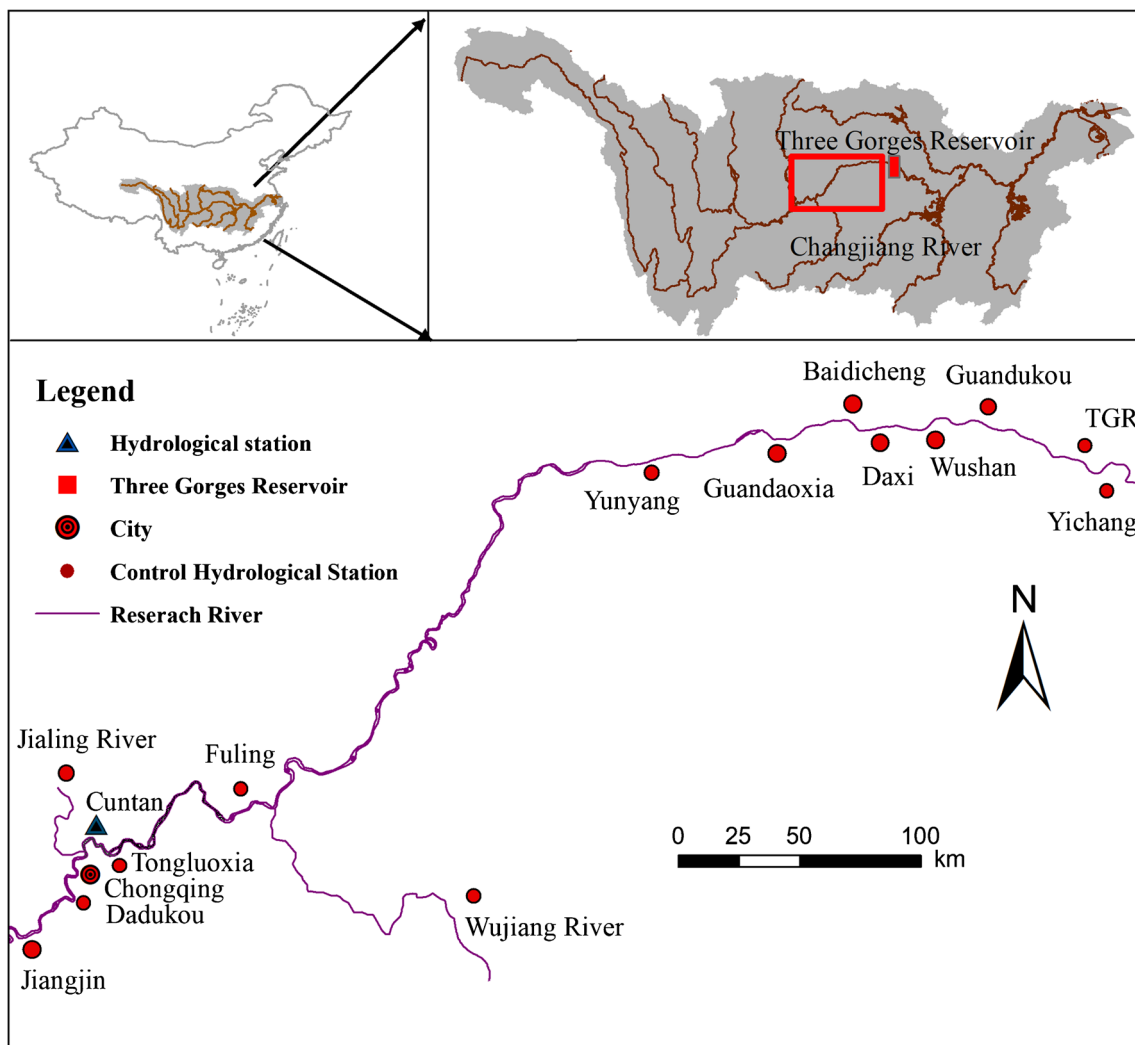
Fig. 1 Backwater area of the Three Gorges reservoir (TGR)

2014; Cheng et al. 2018), and the influence of regulations on downstream navigation (Yan et al. 2019; Yang et al. 2019; Zhang et al. 2019). Compared with the existing downstream research, previous Three Gorges Reservoir (TGR) research focused on the impact of channel siltation (Lu et al. 2010; Xiao et al. 2015; Li et al. 2018b) and environmental and land-slip impacts (Yan et al. 2008; Yang et al. 2010; Wolf et al. 2013; Huang et al. 2016; Song et al. 2018), while little attention has been paid to the navigation condition changes in the reservoir area.

With the increasing economic development in China, the Yangtze River waterway has been used to motivate the construction of the Yangtze river economic zone, called the "Golden Waterway" (Cao et al. 2010). Although the impoundment of the reservoir in a watershed directly increased the waterway depth in the reservoir area, reservoir sedimentation is a global concern as sediment retention can reduce reservoir capacity and navigation depth (Li et al. 2018b). After the first 15 years of operation, sedimentation in the TGR reached 1.59 billion tons (CWRC 2019), 92% of which accumulated in the permanent backwater area (PBA). Moreover, the serious siltation of fine-grained sediments has a potential negative influence on the channel dimensions (Xiao et al. 2015). Further, although the fluctuating backwater area (FBA) presents a scouring pattern, the bed load behavior and limited deposition in some river sections have significantly influenced the navigation depth (Xiao et al. 2019b). Currently, there are few preliminary studies that discuss the interaction of multiple factors, such as water-sediment discharge, reservoir sedimentation, and sediment mining, in response to the sustainability of the navigation conditions in the TGR (Wang et al. 2016).

This study aims to investigate changes in the navigation conditions after the operation of the TGD. Using water-sediment data from the major hydrological stations along the TGR and the river bed level collected from 2003 to 2018, we evaluate the factors responsible for navigation condition changes in the FBA and PBA, and analyze the influence factors of water-sediment discharge, reservoir sedimentation, and sediment mining on the sustainable development of navigation conditions in the TGR.

Table 1 Monthly maintenance waterway depth in the Three Gorges reservoir (TGR)

Reach section	Maintenance waterway depth(m)											
	Jan.	Feb.	Mar.	April	May	June	July	Aug.	Sept.	Oct.	Nov.	Dec.
Dam to Fuling	4.5											
Fuling to Chongqing	4.5	4.0	3.5	3.5	3.5	3.5	4.0	4.0	4.0	4.0	4.5	4.5
Chongqing-Jiangjin	2.9	2.9	2.9	2.9	3.2	3.5	3.7	3.7	3.7	3.5	3.2	2.9

Changes in navigation conditions after TGD operation

Since the 175-m pilot retention stage was realized in 2008, the navigation dimensions of the TGR significantly improved. In particular, the annual maintenance waterway depth increased from 2.9 to 4.5 m in the PBA, and in the FBA, the minimum maintenance waterway depth from Fuling to Chongqing and Chongqing to the Jiangjin reach increased from 2.9 and 2.7 m in 2003 to 3.5 and 2.9 m, respectively, in 2018. The details of the monthly maintenance waterway dimension are listed in Table 1.

Navigation problem in the PBA

From 2003 to 2018, the sedimentation in the PBA was 1.5575 billion m^3, of which the median grain size D50 was 0.002–0.004 mm (IRTCES 2019). As illustrated in Fig. 2 a, the fine-grained deposition along the PBA is obvious, annual deposition density decreased with time, and the most intense deposition occurred in the TGD channel from Guandaokou and Baidicheng to Guandaoxia. Variations in the thalweg from the TGD to the Fuling reach are shown in Fig. 2 b. The fluctuating range of the bed level reaches 62 m near the dam area. Compared with the variation in the water level along the reservoir when the pool level decreased to 145 m, the waterway depth is more than 10 m below and less than 5 m above the Zhongxian river reach. This implies that the navigation problem in the PBA is the result of the fine sediment deposits above the Zhongxian river section. The Huanghuacheng channel, located 350 km upstream from the TGD, deposited 155 million m^3 during the study period, and its maximum deposition thickness reached 50 m (Xiao et al. 2019a).

The scour/deposition distribution in the Huanghuacheng channel is shown in Fig. 3 a. The accumulated sedimentation resulted in a continuous expansion of the side bars toward the main channel, and a gradual decrease in its effective waterway dimension. The river pattern of the Huanghuacheng channel is basically meandering, wherein a central gravel bar becomes exposed during low flows. The left branch of the channel experiences serious siltation, leading to navigational changes for ships traveling upstream from the original left flow route to the right flow route during the flood season (Fig. 3b).

Navigation problems in the FBA

The FBA eroded 0.074 billion m^3 after the operation of the TGD, and its scour/sedimentation density is shown in Fig. 4 a. Considering the influence of the TGR, the annual erosion density increased with increasing distance from the TGD (Fig. 4b). During the falling stage, when the pool level reduces from 175 to 145 m (April–June), the FBA transfers to the natural channel, stopping TGD control. Meanwhile, with rapidly decreasing water levels along the reservoir, water power increases trigger a bed load transport peak, leading to temporary deposition in some river sections.

The Qingyanzi channel, located 565 km upstream from the TGD, exhibits a scouring pattern and was eroded by 10.51 million m^3 from 2003 to 2018. The scour/deposition distribution between February 1 and June 30 in 2017 is shown in Fig. 5 a. Note that a few gravel deposition areas remain located in the main channel, causing a decrease in the waterway depth. As shown in Fig. 5 b, the waterway depth clearance is only 0.5 m and is sensitive to deposition thickness, implying that shipping risk increases when the pool level is below 149 m in the falling stage.
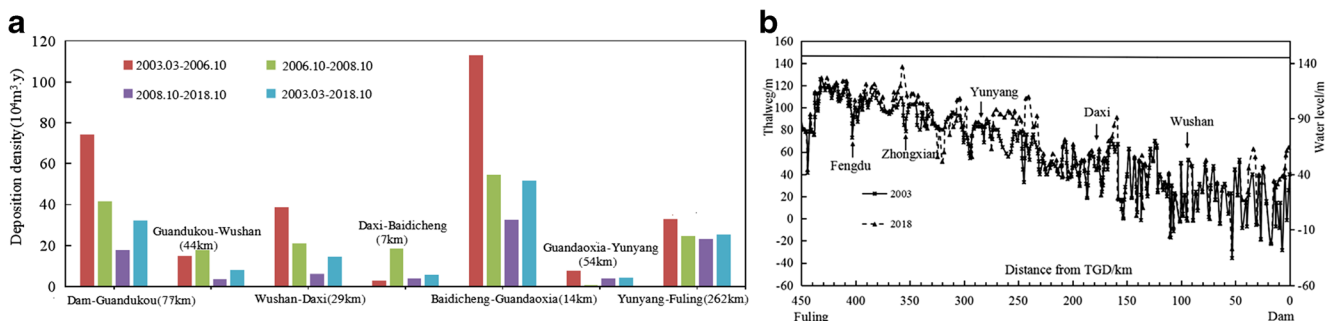
Fig. 2 Changes in the (**a**) annual deposition density and (**b**) thalweg of the permanent backwater area (PBA)
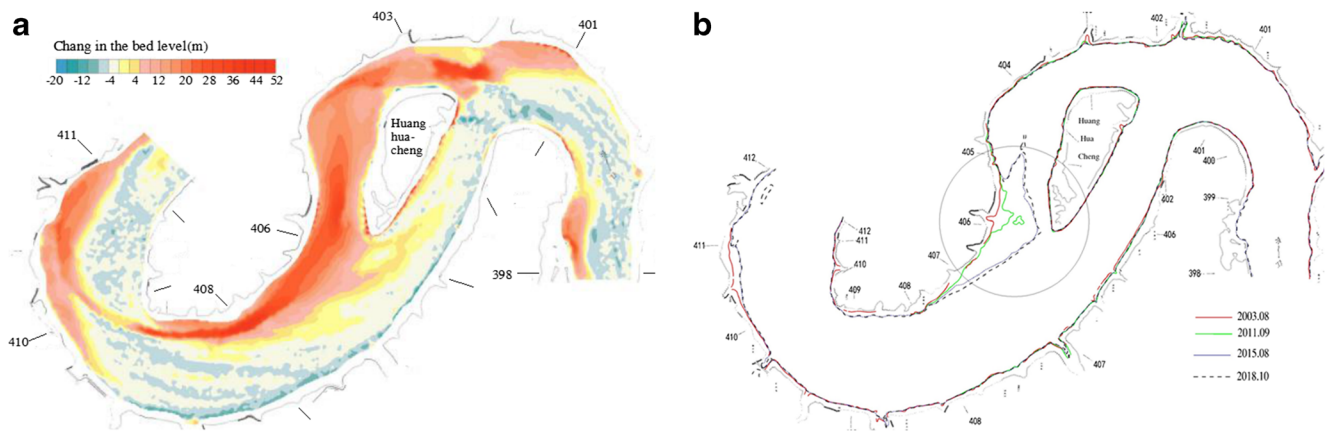
Fig. 3 Changes in the (**a**) river bed level and (**b**) lowest navigable water level of the Huanghuacheng river reach

The amount of the sediment scour in the Changshou channel which is located 580 km upstream from the TGD, is not obvious, reaching approximately 1.31 million m^3, and its deposition location is in the entrance of the right branch (Fig. 6a). In its falling stage, the water level changes with time, implying that miniscule sedimentation influences the navigation clearance, increasing shipping risks (Fig. 6b). The Luoqi channel, located 599 km upstream from the TGD, was eroded by 8.21 million m^3 from 2003 to 2018. It contains some steep-walled excavation pits near the channel boundary, of which the depth of these pits reach 22m (Fig. 7a). By comparing the navigable water level during the falling stage with that of the borrow pits and that prior to the sediment mining, it was found that the channel water level decreased, tending to maintain the minimum waterway level (Fig. 7b). This result reveals that uncontrolled gravel excavation could lead to a negative effect on navigation conditions.

Influencing factors on TGR navigation conditions:methods

Regarding navigation condition changes in the TGR, the main navigable problems in the PBA and FBA are related to fine grained sedimentation, bed load behavior, and sediment mining. Inlet water-sediment discharge is useful in determining sediment transport and river bed deformation. To investigate the change in the waterway dimension of the TGR, the Mann-Kendall (M-K) test and rescaled range (R/S) analysis were employed to predict the trends of the runoff and sediment discharge. Then, a 2D hydro-sediment numerical model was used to evaluate the impact of bed load behavior and sediment mining on navigation conditions in the FBA.

Mann-Kendall test and R/S analysis

The M–K test and rescaled range (R/S) analysis have typically been used to detect the temporal–spatial distributions of the variations in annual runoff–sediment transport and their changing trends (Yue et al. 2002). The details of the methods are fully described in Xiao et al. (2019a).

The 2D hydrological-sediment transport numerical model

Description of 2D numerical model

The 2D numerical model applied herein incorporates hydrodynamic, sediment transport, and morphodynamic sub-models.
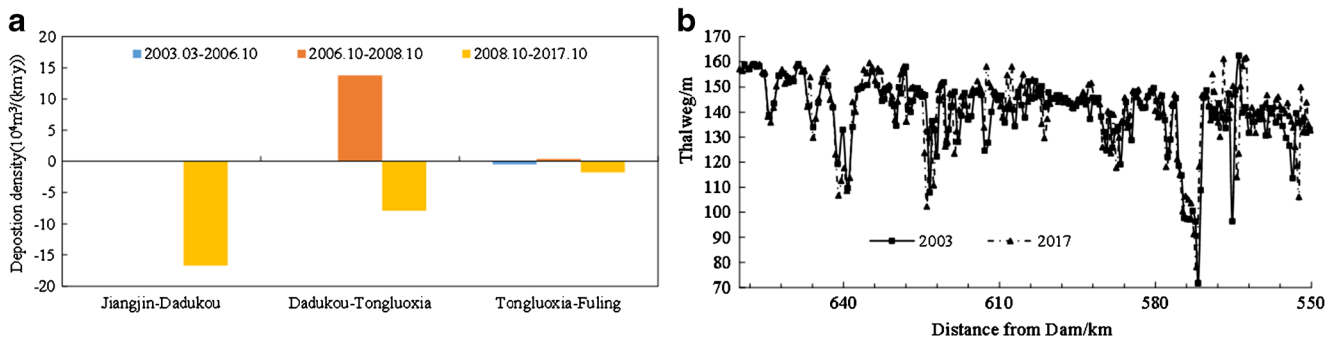
Fig. 4 Changes in the (**a**) deposition density and (**b**) thalweg of the fluctuating backwater area (FBA)
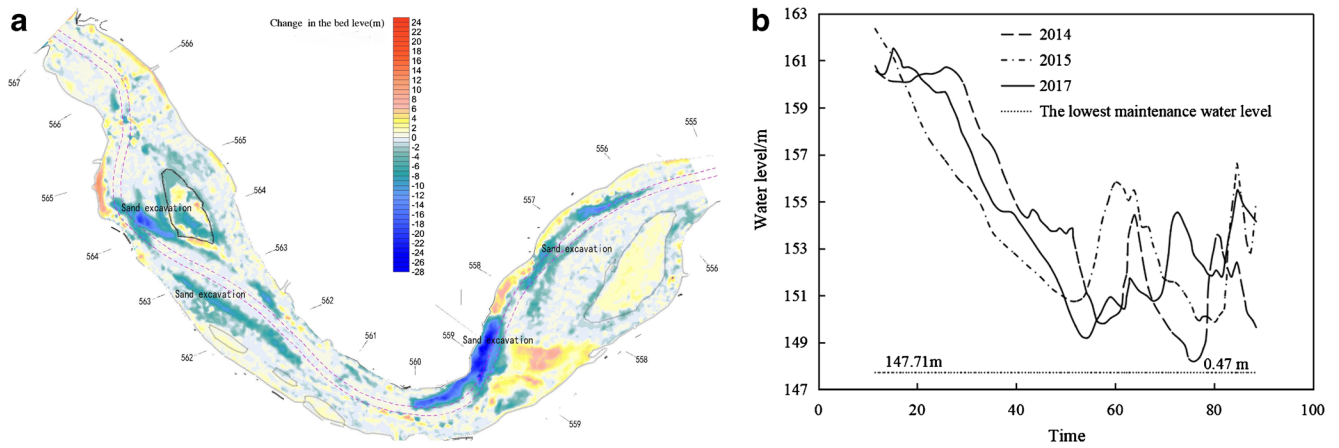
Fig. 5 Changes in the (**a**) river bed level and (**b**) water level versus the lowest maintenance water level in the Qingyanzi channel

The hydrodynamic sub-model solves the Reynolds averaged Navier-Stokes mass and momentum conservation equations in an orthogonal curvilinear grid system as follows (Xiao 2013):

$$\frac{\partial z}{\partial T} + \frac{1}{J}\left[\frac{\partial(h_2 q)}{\partial \xi} + \frac{\partial(h_1 p)}{\partial \eta}\right] = 0 \tag{1}$$

$$
\begin{aligned}
&\frac{\partial q}{\partial t} + \beta\left(\frac{1}{J}\frac{\partial(h_2 qU)}{\partial \xi} + \frac{1}{J}\frac{\partial(h_1 pU)}{\partial \eta} - \frac{pV}{J}\frac{\partial h_2}{\partial \xi} + \frac{qV}{J}\frac{\partial h_1}{\partial \eta}\right) - fp + \frac{gH}{h_1}\frac{\partial Z}{\partial \xi} + \frac{qg|\overline{q}|}{(CH)^2} \\
&= \frac{\nu_e H}{h_1}\frac{\partial E}{\partial \xi} - \frac{\nu_e H}{h_2}\frac{\partial F}{\partial \eta} + \frac{1}{J}\frac{\partial(h_2 D_{11})}{\partial \xi} + \frac{1}{J}\frac{\partial(h_1 D_{12})}{\partial \eta} + \frac{1}{J}\frac{\partial h_1}{\partial \eta}D_{12} - \frac{1}{J}\frac{\partial h_2}{\partial \xi}D_{22} \\
&\frac{\partial p}{\partial t} + \beta\left(\frac{1}{J}\frac{\partial(h_2 qV)}{\partial \xi} + \frac{1}{J}\frac{\partial(h_1 pV)}{\partial \eta} + \frac{pU}{J}\frac{\partial h_2}{\partial \xi} - \frac{qU}{J}\frac{\partial h_1}{\partial \eta}\right) + fq + \frac{gH}{h_2}\frac{\partial Z}{\partial \eta} + \frac{pg|\overline{q}|}{(CH)^2} \\
&= \frac{\nu_e H}{h_2}\frac{\partial E}{\partial \eta} + \frac{\nu_e H}{h_1}\frac{\partial F}{\partial \xi} + \frac{1}{J}\frac{\partial(h_2 D_{12})}{\partial \xi} + \frac{1}{J}\frac{\partial(h_1 D_{22})}{\partial \eta} - \frac{1}{J}\frac{\partial h_1}{\partial \eta}D_{11} + \frac{1}{j}\frac{\partial h_2}{\partial \xi}D_{12}
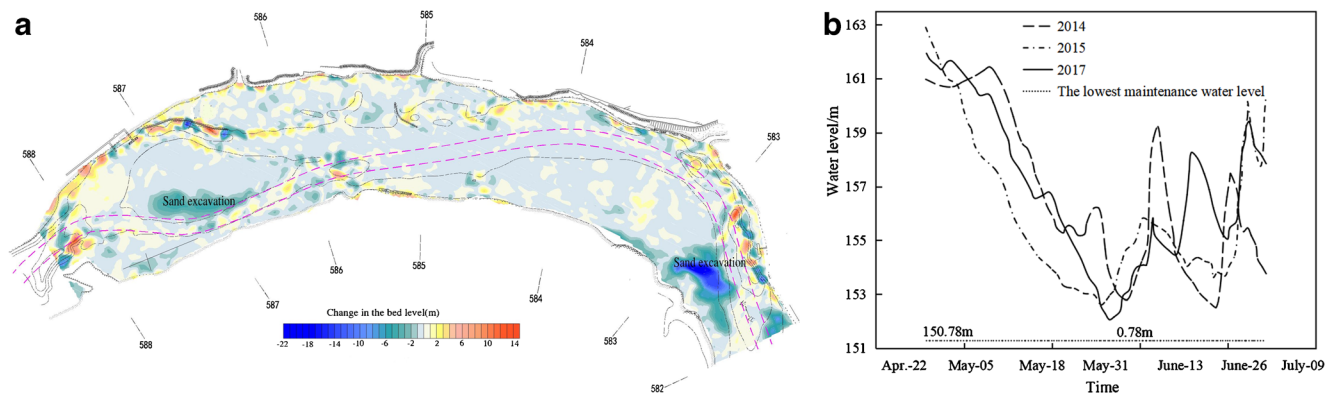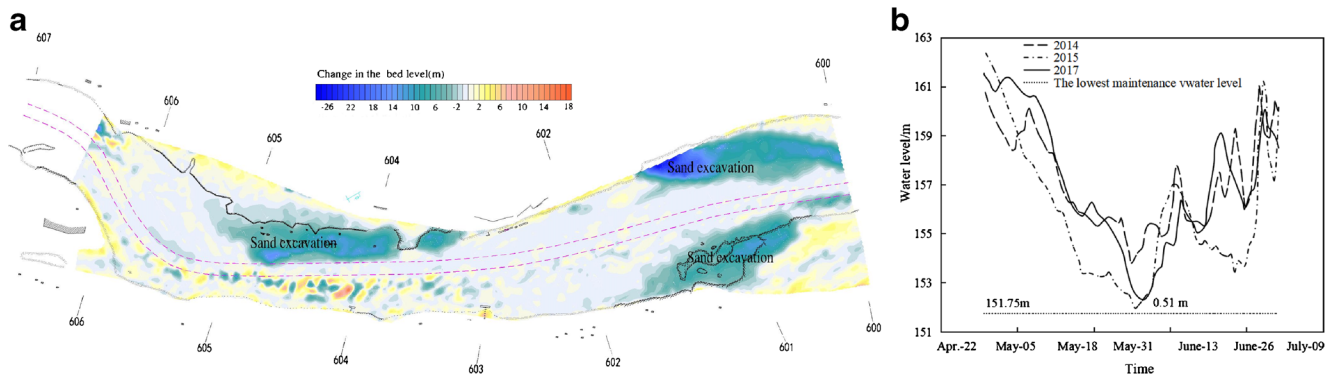\end{aligned}
\tag{2}
$$

Fig. 6 Changes in the (**a**) river bed level and (**b**) water level versus the lowest maintenance water level in the channel of Changshou

Fig. 7 Changes in the (**a**) river bed level and (**b**) water level versus the lowest maintenance water level in the channel of Luoqi

where:

$$E = \frac{1}{J}\left[\frac{\partial(h_2 U)}{\partial \xi} + \frac{\partial(h_1 V)}{\partial \eta}\right], \quad F$$

$$= \frac{1}{J}\left[\frac{\partial(h_2 V)}{\partial \xi} - \frac{\partial(h_1 U)}{\partial \eta}\right] \tag{3}$$

in which ξ and η are orthogonal curvilinear coordinates, h_1 and h_2 are the lame coefficients, U and V are the depth-averaged velocity components in the ξ and η directions of curvilinear coordinate, respectively, and the flow discharge components/unit width are $\vec{q} = (q, p) = (UH, VH)$. Further,

Z is the water level based on the reference datum, β is the correction coefficient considering the non-uniform vertical velocity, f is Coriolis coefficient, g is the acceleration of gravity, C is the Chezy coefficient, υ_e is the depth-averaged vortex viscosity, Z_s and Z_b are the water and bed elevation, respectively, and D_{11}, D_{12}, D_{21}, and D_{22} are the depth-averaged dispersion stress terms that consider the secondary flow.

The sediment transport sub-model includes the non-equilibrium suspended-load and bed-load transport equations, written as (Xiao et al. 2014, 2015):

$$\frac{\partial(HC_k)}{\partial t} + \frac{1}{J}\left[\frac{\partial(HC_k U h_2)}{\partial \xi} + \frac{\partial(HC_k V h_1)}{\partial \eta}\right] - \frac{1}{J}\left[\frac{\partial}{\partial \xi}\left(H\varepsilon_\xi \frac{h_2}{h_1}\frac{\partial C_k}{\partial \xi}\right) + \frac{\partial}{\partial \eta}\left(H\varepsilon_\eta \frac{h_1}{h_2}\frac{\partial C_k}{\partial \eta}\right)\right] + \alpha_k \omega_k (C_k - C_{*k}) = 0 \tag{4}$$

$$\frac{1}{\overline{U}}\frac{\partial(q_{bk})}{\partial t} + \frac{1}{J}\left[\frac{\partial(h_2 \alpha_{b\xi} q_{bk})}{\partial \xi} + \frac{\partial(h_1 \alpha_{b\eta} q_{bk})}{\partial \eta}\right] + \frac{1}{L}(q_{bk} - q_{b*k}) = 0$$

where subscript k indicates the size group, C_k and C_{*k} are the depth-averaged suspended load concentration and transport capacity of the kth size group, respectively (the value of C_{*k} is provided in Xiao et al. (2015)), ε_ξ, ε_η are the depth-averaged longitudinal and transverse diffusivity coefficients of the sediment, respectively, k_l and k_t are the longitudinal and transverse components of the depth-averaged diffusivity coefficient, respectively, ω_k denotes the fall velocity of the kth size group, q_{bk} is the bed load transport rate for the kth size group, $\overline{U}$ is the depth-averaged velocity, $\alpha_{b\xi}$, $\alpha_{b\eta}$ are the projections of the ξ, η directions, respectively, and q_{b*k} is the kth size group transport capacity for equilibrium transport.

Bed deformation can be calculated using the overall mass balance equation for the sediment as follows (Xiao et al. 2014):

$$\sum_{k=1}^{N}\frac{1}{1-\lambda}\cdot\frac{\partial Z_k}{\partial t} + \sum_{k=1}^{N}\frac{1}{J}\left[\frac{\partial h_2 \alpha_{b\xi} q_{bk}}{\partial \xi} + \frac{\partial h_1 \alpha_{b\eta} q_{bk}}{\partial \eta}\right]$$

$$+ \sum_{k=1}^{N}\alpha_k \omega_k (C_k - C_{*k})$$

$$= 0 \tag{5}$$

where Z_k is the thickness of the sediment layer and a_k is the saturation recovery coefficient for size group k.

The numerical solution is based on the Beam and Waring alternating-direction implicit (ADI) scheme, of which the basic source code and solution process is provided in Xiao (2013). The verification of the 2D hydrological sediment numerical model includes the fluvial process of the physical meandering channel, the TGD downstream, and the PBA in
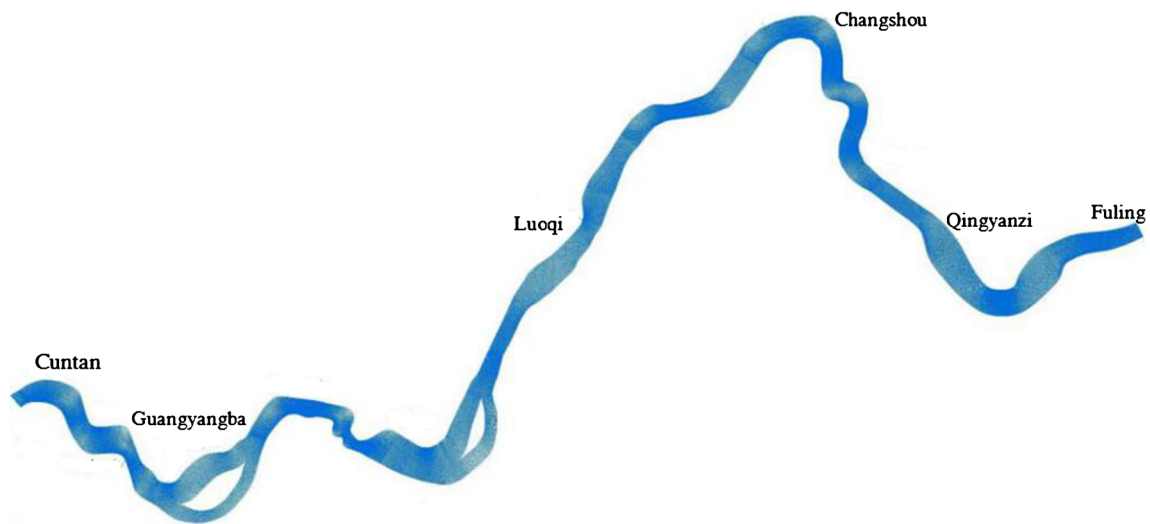
Fig. 8 Computational domain and mesh from Chongqing to the Fuling reach in the fluctuating backwater area (FBA)

the TGR. Additional details on numerical model application can be found in Xiao et al. (2014, 2015, 2016).

Verification of the 2D numerical model in the FBA

After TGD pool level rose to 175 m in 2008, the 232-km-long fluctuating backwater zone stretched from Fuling to Jiangjin. As the study area is slightly meandering (Fig. 1), an orthogonal curvilinear coordinate system was applied to 3255 × 60 grids in the computational domain with a time interval of t = 8 s. The grid spacing in the ξ and η directions are 20–30 m and 15–20 m, respectively (Fig. 8). The river bed level in October 2009 was taken as the initial topography. From 2009 to 2016, the observed daily water discharge at the Cuntan station and the water level at the Qingxichang station were used as the inlet and outlet boundary conditions, respectively (CWRC 2017). The range of the sand grain size along the FBA is 0.157–0.238 mm, wherein a median grain size of D_{50} was adopted for simulation (Table 2). Based on the composition of the bed material in each river section, the gravel bed load calculation was divided into four groups ranging in diameter from 12 to 90 mm (Table 3). A real time period of ten years was selected, and the simulation results of water level, flow velocity, and river bed level changes were compared with the measured data for validation.

The calculated water levels at the measured control hydraulic stations in the FBA were in agreement with the field measurements from September 2009 to December 2016 (Fig. 9).The relative error at the 2 reference stations was < 0.06 m under various discharges. Further, the observed and simulated cross-sectional distributions of the depth-averaged velocity at typical cross sections are shown in Fig. 10. The velocity performance was found to be slightly higher than that of the measured value at the meandering river section, which contributed to the accuracy of the secondary current simulation. This discrepancy decreased with decreasing sinuosity, wherein the maximum deviation was less than 0.08 m/s. These results indicate that the 2D numerical model can reproduce the flow pattern in the FBA and support the sediment transport process simulation findings.

The amount of sedimentation in the Qingyanzi, Changshou, and Luoqi river sections (Table 4) shows that the total sediment deposit deviation was below 25%. Moreover, the simulated maximum deposition thicknesses were 3.16 m, 0.87 m, and 0.67 m, which is only 69%, 79%, and 77% of the observed values in the Luoqi, Changshou, and Qingyanzi channels, respectively. These deviations may result from the uncertainty of the sediment supply and bed material. A comparison of the calculated and observed deposition patterns in these channels showed that the simulated sedimentation is smaller than that of the field observations.

Table 2　Median sand grain size (D_{50})

Year	2009	2010	2011	2012	2013	2014	2015	2016
D_{50} (mm)	0.262	0.178	0.143	0.138	0.160	0.154	0.147	0.152

Table 3　Fraction of gravel bed load in simulation

Group	1	2	3	4
D (mm)	12	22	45	90
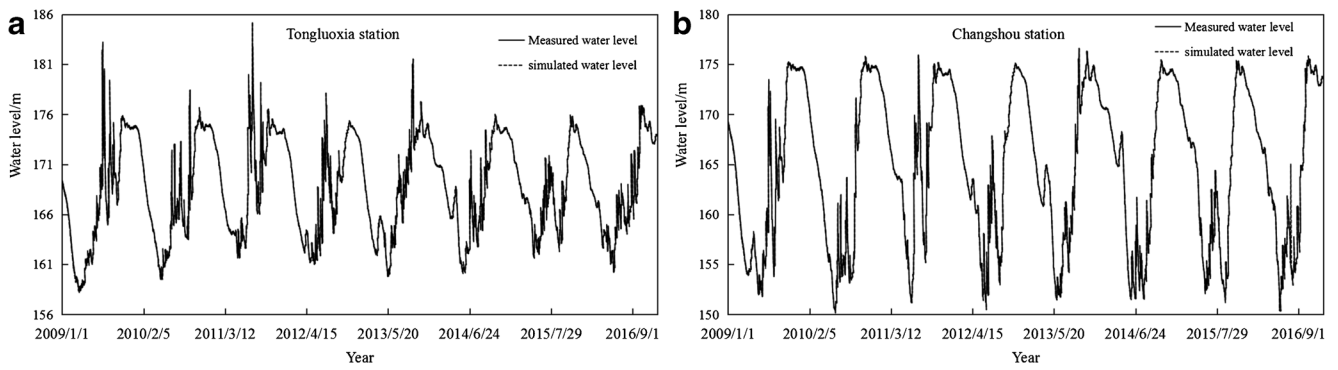
Fig. 9 Calculated and measured water levels along the reaches in the fluctuating backwater area (FBA) of the Three Gorges reservoir (TGR)

Moreover, a comparison of changes in the bed topography between the simulated and measured data indicated that the calculated scour and deposition distributions are in agreement with those observed in the Luoqi, Changshou, and Qingyanzi river sections (Figs. 6, 7, 8, and 11). However, the maximum deposition thickness was 2.5 m, which is smaller than the field measurements, reaching only 85% of the observed value. This finding underestimates the influence of sediment mining activity. A comparison of changes in the bed level at typical cross sections showed that with increasing time, the cross-section patterns became measurements with acceptable ranges of error (Fig. 12). Thus, the 2D numerical model can predict the variation in the river bed level with reasonable agreement with the measured data.
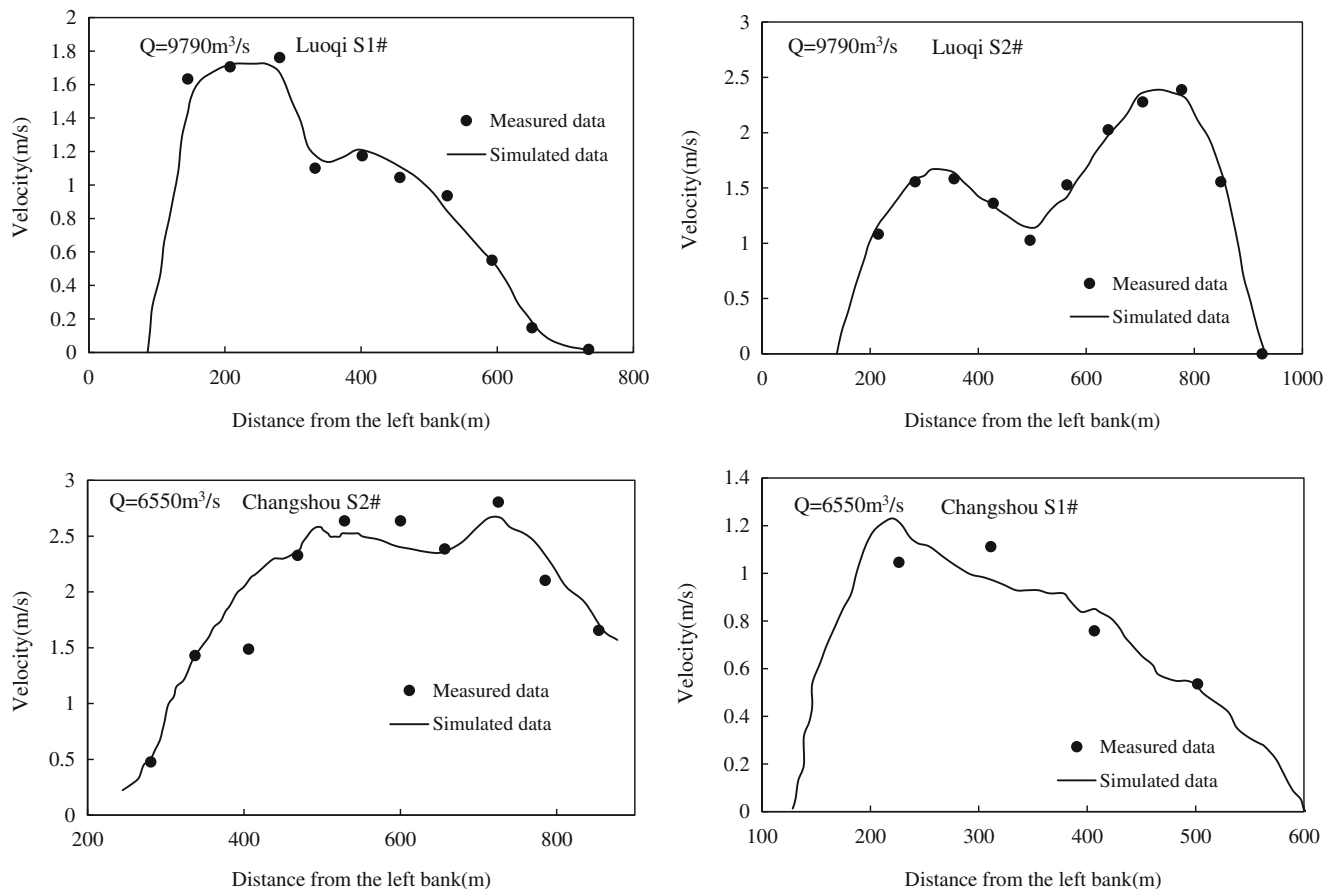
Fig. 10 Measured and calculated distributions of flow velocity over a typical cross-section

Table 4 Comparison of the deposition volumes during 2009 to 2016

| Channel	Measured maximum deposition thickness (m)	Simulated maximum deposition thickness (m)	Measured volume (10^4 m^3)	Calculated volume (10^4 m^3)
Luoqi	4.6	3.16	11.6	9.53
Changshou	1.21	0.87	10.8	8.94
Qingyanzi	2.01	0.67	57.2	44.6

Results and discussion

Variations in TGR water-sediment discharge

The TGR control hydraulic station is the Cuntan station (Fig.1). Considering the sediment characteristics for deposition in the backwater area, the measured sediment transport data were divided into suspended, sand, and gravel bed loads. The dataset of the daily water discharge and sediment supply is provided in Sediment-Panel (2018). Xiao et al. (2019a) used an M-K test and R/S analysis to obtain the UF-UB and R/S curves for the mean annual runoff-suspended load discharge from 1954 to 2017 at the Cuntan station. Their results showed that the decreasing trend of inlet flow discharge is not significant, and the decline of the fine-grained sediment supply would alleviate the sedimentation process in the PBA. The change of deposition density versus fine-grained sediment supply for the Huanghuacheng channel is shown in Fig. 13. Its results imply that the sedimentation tends to stabilize with decreasing annual suspended load supply, thereby contributing to safe navigation conditions in the PBA.

Temporal variations in sand and gravel bed loads at the Cuntan station from 1991 to 2017 (Fig. 14) showed an overall declining pattern. In particular, the UF values of sand discharge were less than 0, indicating that its
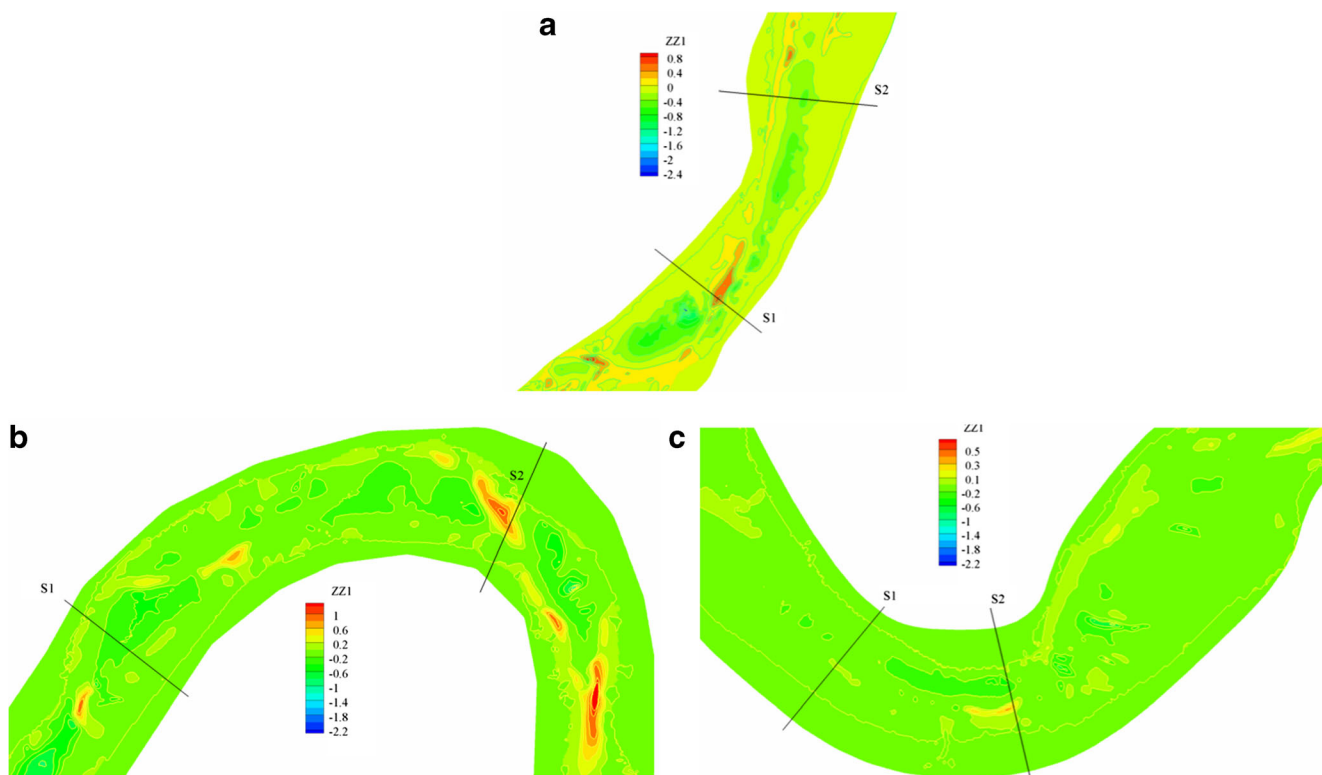
Fig. 11 Calculated and measured scour/deposition changes in typical channels: **a** Qinyanzi, **b** Changshou, and **c** Luoqi river sections

decrease is slight, and would be maintained after 2005. A significant decrease in gravel bed load occurred in 2003, and the UB values were greater than 0 after 2011, implying that a slight increase took place between 2011 and 2012. Then, the fluctuating range decreased and maintained the present level. The changing trends of the sand and gravel bed loads at the control station (Fig. 15) have H values of 1.19 and 1.12, respectively,
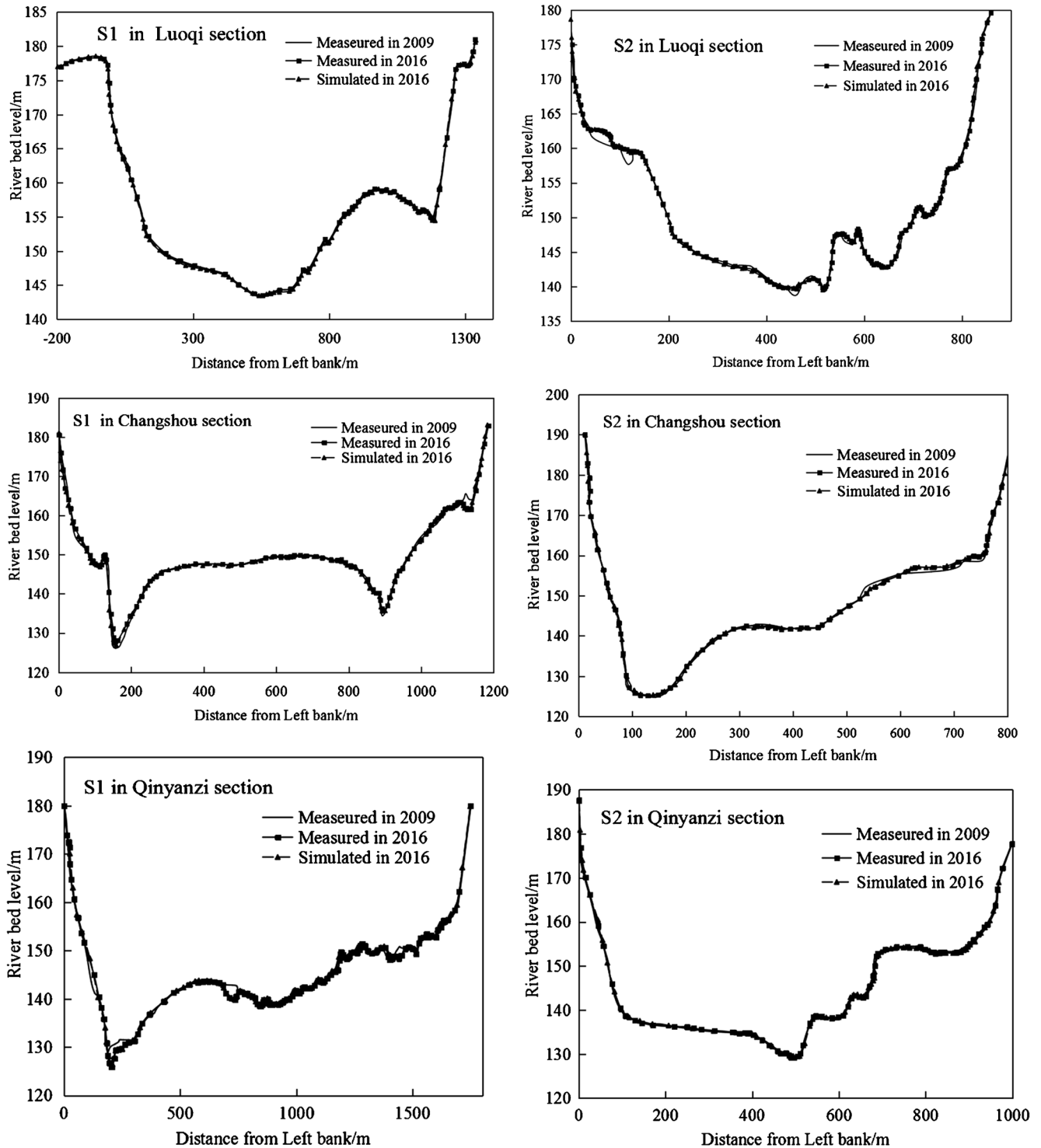

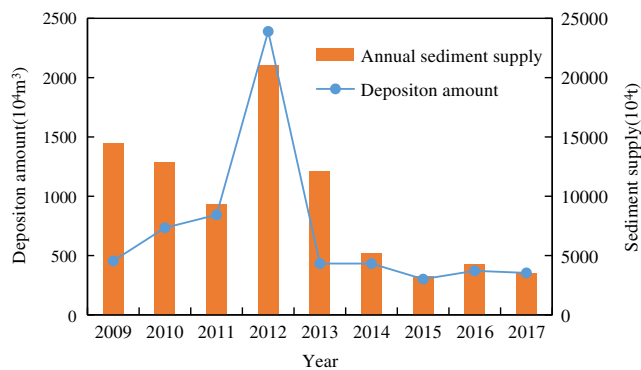Fig. 12 Calculated and measured scour/deposition changes in typical cross sections

Fig. 13 Changes in the deposition in the Huanghuacheng channel with varying sediment supply

demonstrating that their decline would remain at the current levels. Although the bed load discharge decline decreases, to some extent, deposition in the FBA,

temporary bed load deposition, and transport during the falling stage should be further examined regarding waterway depth clearance.

Analysis of bed load behavior in the navigation-obstructing channels in the FBA

Changes in the water-sediment discharge of the TGR show that, in 2012, there was a high water-sediment discharge process, which negatively influenced navigation conditions. In this study, the sedimentation process was reproduced to investigate the navigation obstructing time and its response to the flow discharge conditions with increasing sediment supply. The bed topography of the FBA in 2012 was set as the initial condition, and the water discharge, sediment supply, and water level at the control stations from 2012 to 2013 were
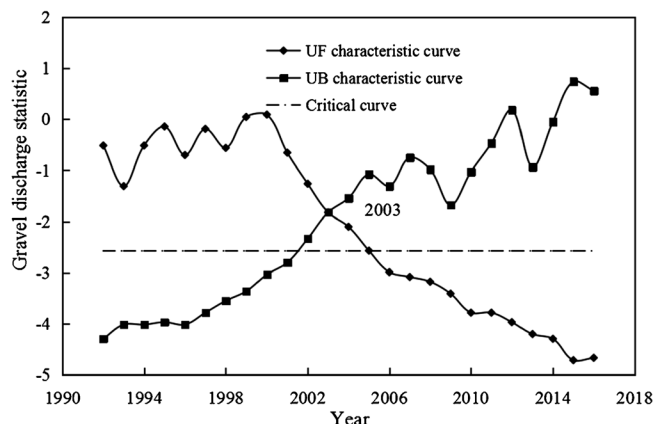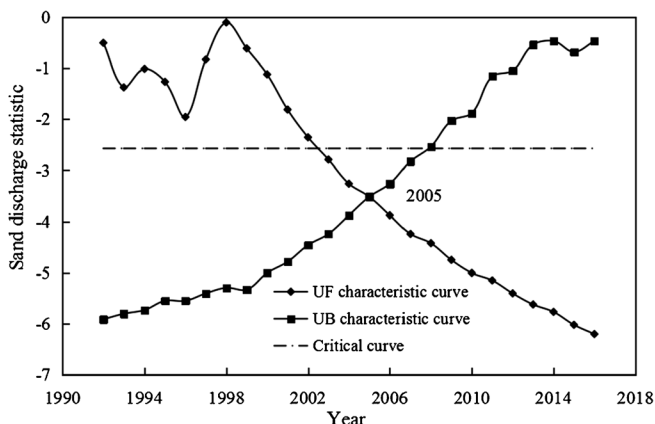

Fig. 14 UF-UB curve of sand and gravel supply at the Cuntan station. **a** Change in sand discharge and **b** change in gravel load discharge
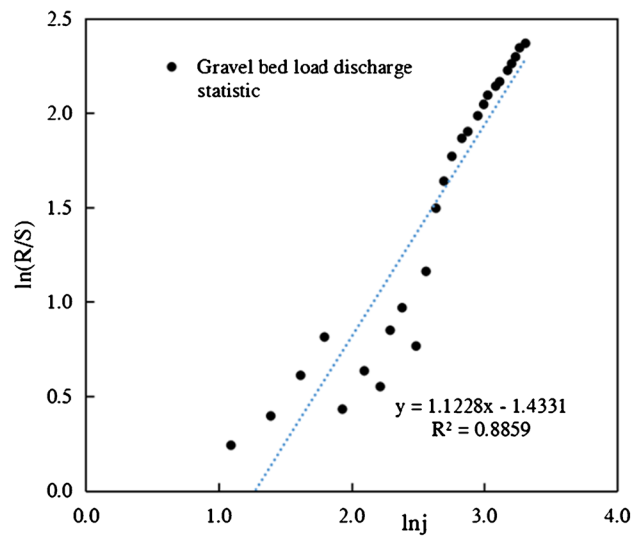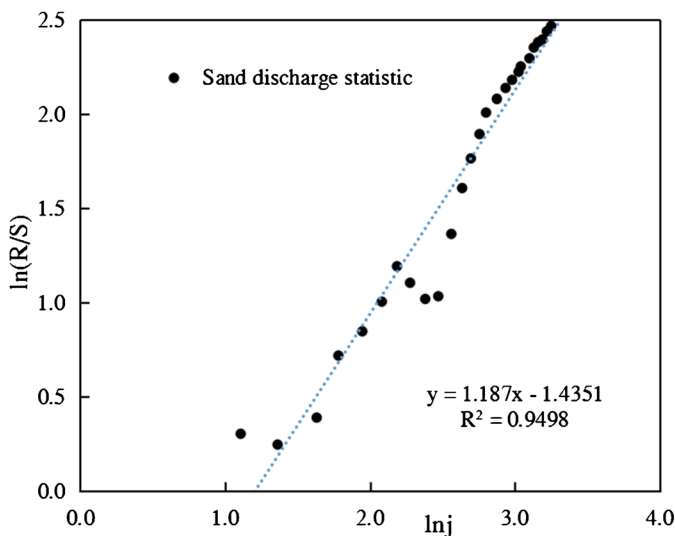

Fig. 15 R/S curve of sand and gravel supply at the Cuntan station. Change trends of (**a**) sand discharge and (**b**) gravel load discharge

Table 5 The sedimentation process during a high water-sediment discharge year

Channel	01/2012–05/2012 (10^4 m³)	06/2012–09/2012 (10^4 m³)	10/2012–03/2013 (10^4 m³)	Averaged deposition depth (m)
Luoqi	13.86	27.93	36.15	0.064
Changshou	0.875	8.694	13.992	0.04
Qingyanzi	5.763	10.46	12.09	0.037

adopted as boundary conditions. Note that the other simulation parameters were the same as those in the verification case.

The amounts of sediment deposition in the navigation-obstructing channels are summarized in Table 5. The deposition patterns of the Luoqi, Changshou, and Qingyanzi channels in a typical year revealed that sediment deposition reached 1.385×10^5 m³, 0.875×10^4 m³, and 5.763×10^4 m³ after the falling stage, respectively. Then, sedimentation density increased with increasing water-sediment supply, reaching 27.89×10^4 m³, 8.6945×10^4 m³, and 10.46×10^4 m³ after the flood season, respectively. During the water retention stage, as the TGD pool level increased, the deposition density decreased to 3.615×10^5 m³, 1.399×10^5 m³, and 1.209×10^5 m³, respectively, before the subsequent falling
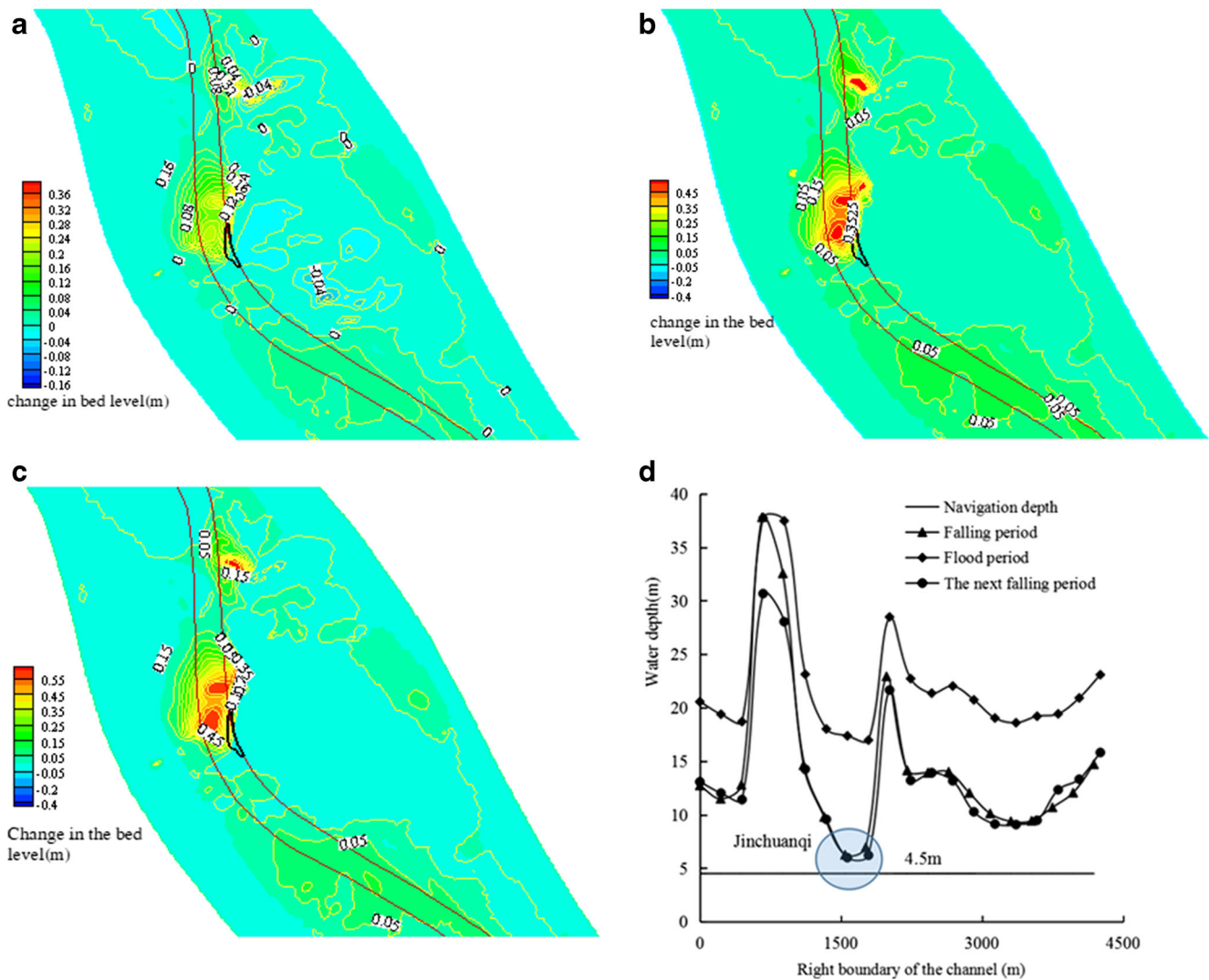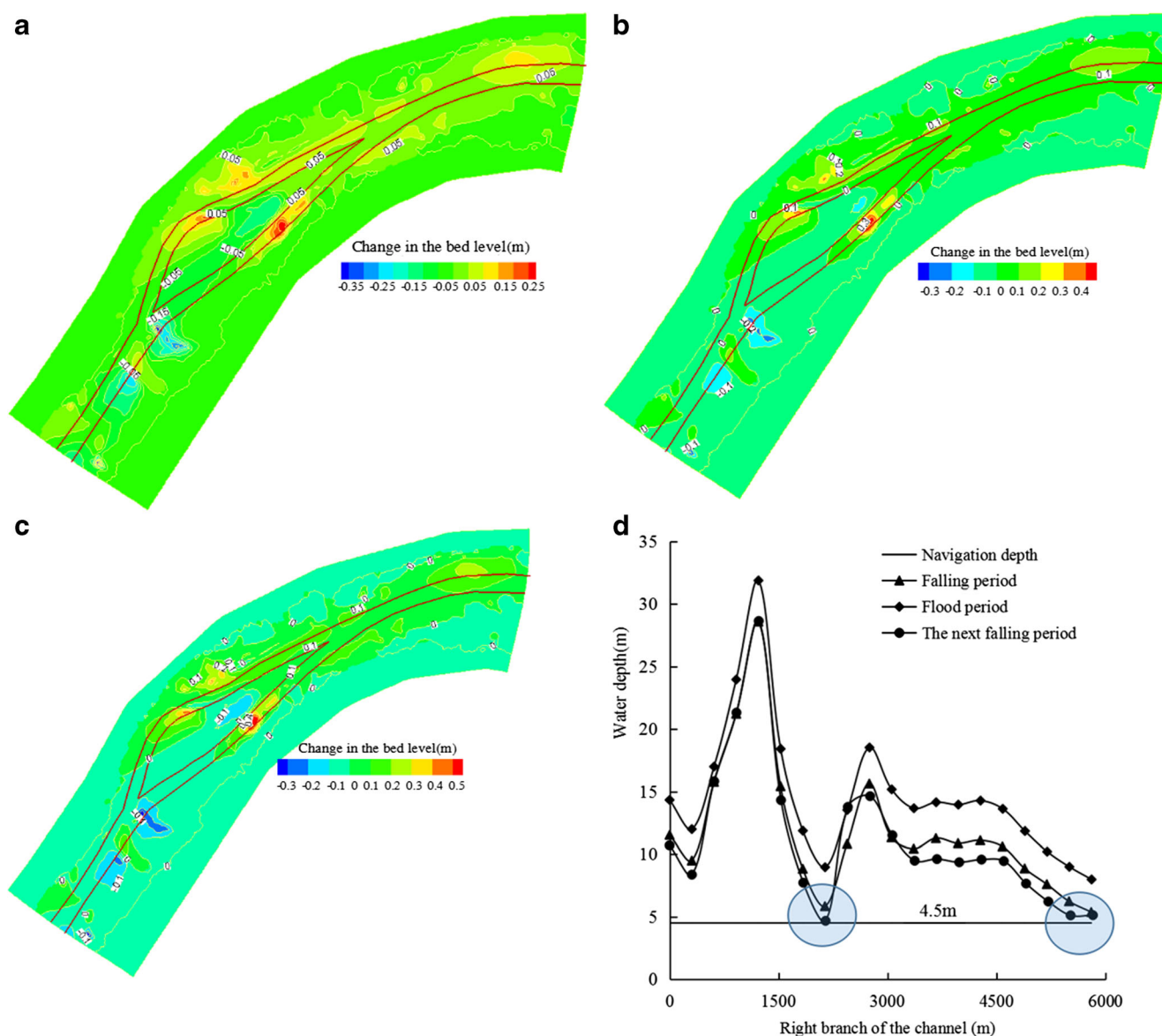

Fig. 16 Deposition process and water level changes during a typical year in the Qinyanzi channel (**a**) after the falling stage, (**b**) after the flood season, (**c**) before the next falling stage, and (**d**) water level variation of the central channel

stage in 2013. Overall, the total averaged deposition depths of these channels were 0.064 m, 0.082 m, and 0.12 m, respectively.

Figure 16 a–c show that the main sedimentation of the Qinyanzi occurs in Jinchuanqi, with its thickness increasing to 0.32 m after the falling stage, 0.53 m after the flood stage, and 0.59 m before the next falling stage with increasing water-sediment supply and time. The water depths along the main channel during its three stages are presented in Fig. 16 d, wherein the navigable water depths are above 8 m during the entire year, with the exception of the right boundary near Jinchuanqi, which is 5.6 m during low flow discharge. These results indicate that the water depth near Jinchuanqi should be of focus during

the subsequent falling stage in order to maintain the safe shipping.

The scour and sedimentation changes in the Changshou channel after the low-flow, high-flow, and water storage periods are shown in Fig. 17 a–c. Overall, the maximum deposition occurred in the navigable boundary of the left branch. Meanwhile, the water depth during the falling period shows that the minimum navigable depth is 6.3 m, which occurs at a maximum deposition of 0.21 m. As the sedimentation depth was only 3.33% of the navigable depth, the influence of deposition on safe navigation can be neglected during this period. After the high-flow period, the sedimentation depth increased to 0.45 m and the average water depth increased to 15 m. Finally, after the water retention stage, the maximum

Fig. 17 Deposition process and water level changes during a typical year in the Changshou channel (a) after the falling stage, (b) after the flood season, (c) before the next falling stage, and (d) water level variation of the central channel

deposition was 0.61 m, and the water depth declined to 4.9 m in the main sedimentation area during the next falling stage (Fig. 17d). This small bed load deposition reduces the navigable depth, negatively impacting the navigation conditions.

Figure 18 shows the changes in the bed topography and the water depth in the central channel during the falling, flood, and water retention stages in the Luoqi river section. A maximum deposition thickness of 0.24 m occurred in the main channel of Xialuoqi (Fig. 18a). The water depth of the channel was greater than 6.5 m during the whole falling stage, implying that navigation was safe. The scour/deposition distribution of the Luoqi channel after the flood season shows that the maximum deposition depth reached 0.46 m (Fig. 18c). However, the water depth increased rapidly to 15 m along the main channel; thus, the influence of sedimentation can

be ignored. The maximum deposition thickness increased to 0.53 m in subsequent falling stage, and the corresponding water depth was 5.8 m (Fig. 18d), indicating that the maintenance depth is sensitive to deposition in the next falling stage after a high water-sediment discharge year.

Influence of sediment mining on TGR navigation conditions

Based on the river bed levels of the TGR in 2007 and 2016, sediment mining activities occurred mainly in the gravel shoals near the river bank of the FBA, especially in the Wumu zhuang-Zhanqizi and Cuntan-Mudong channels (Fig. 19). The total amount of sediment mining reached 1.61×10^4 million m^3 in 2017, and the Guangyangba, Luoqi, Changshou,
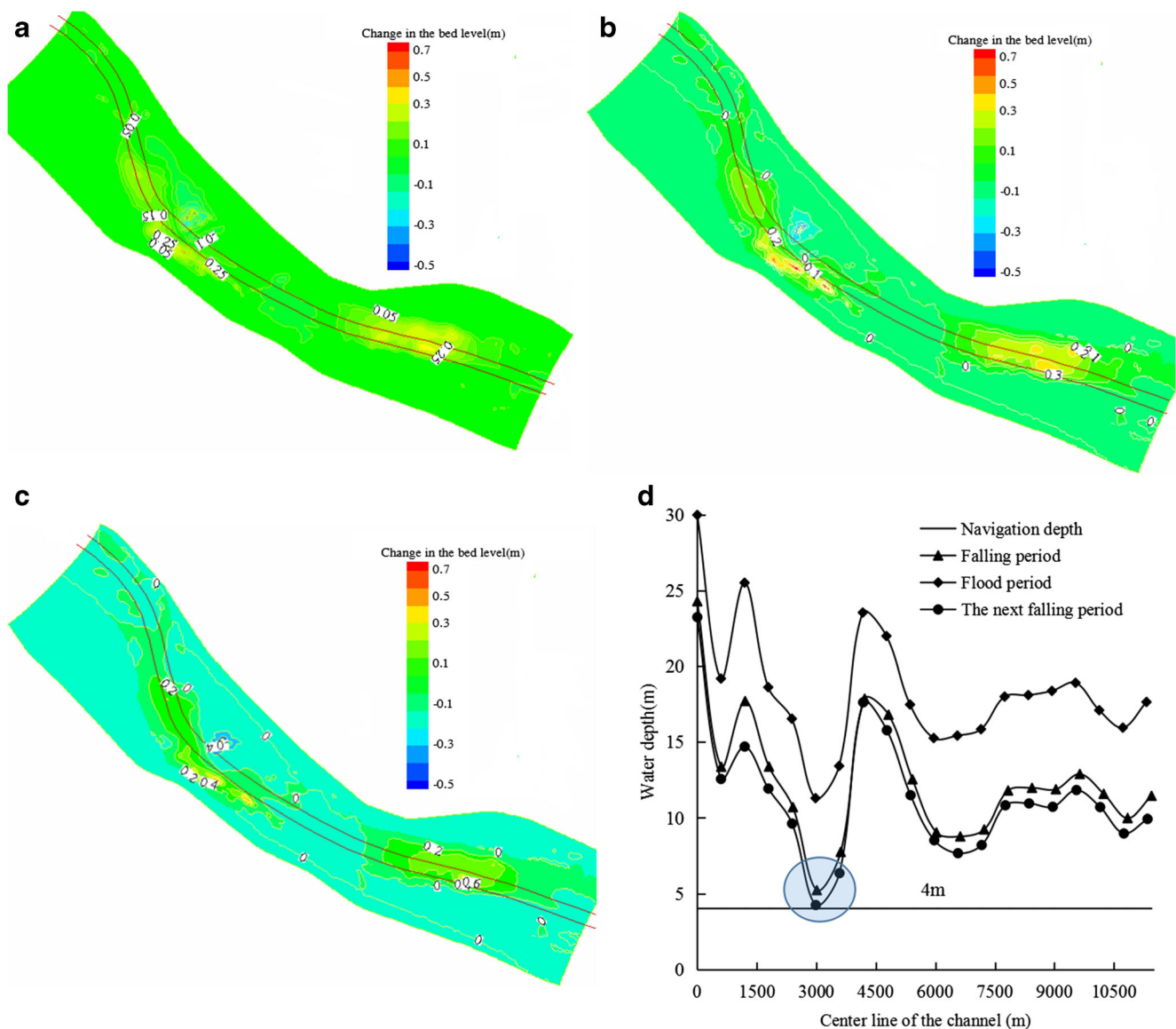
Fig. 18 Deposition process and water level changes during a typical year in the Luoqi channel (a) after the falling stage, (b) after the flood season, (c) before the next falling stage, and (d) water level variation of the central channel
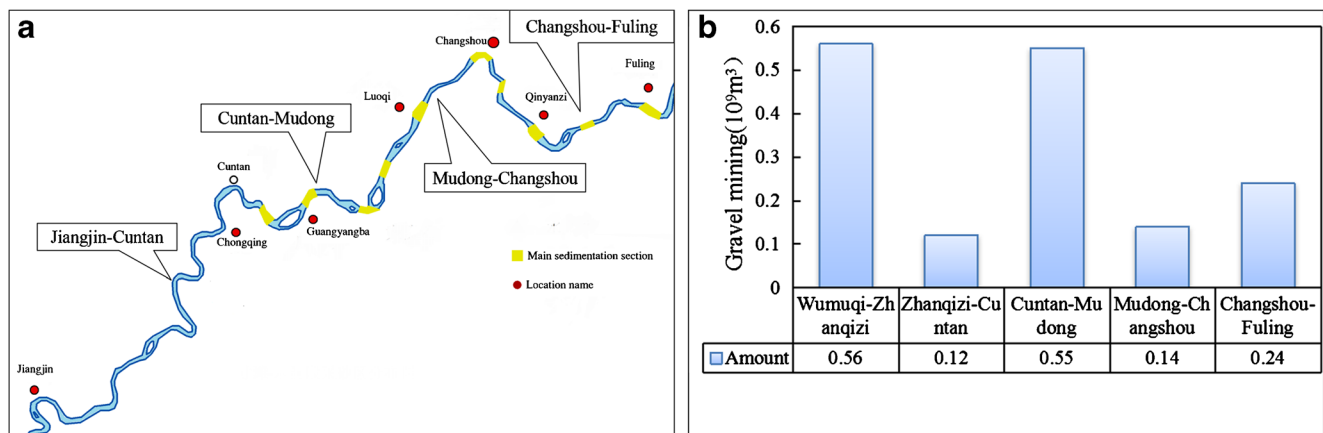
Fig. 19 Distribution of the excavation pits in the fluctuating backwater area (FBA)

and Qinyanzi channels were the main gravel excavation areas in the FBA (Xiao et al. 2019b). Excavation pits can cause increases in water area, decreases in local water levels, and damage bed structures and ecological environments.

For the TGR waterway conditions, the flow patterns under the low, middle, and high flow scenarios were simulated to investigate the impact of the sediment mining on navigable water level in FBA. Two types of topography parameters were adopted herein based on data in 2017. The first type is the bed level considering sediment mining activity, and the other is no sediment extraction. The inlet and outlet boundary conditions of the simulation scenarios are summarized in Table 6.

Figure 20 shows the changes in the water level along the main channels of the Guangyangba, Luoqi, Changshou, and Qinyanzi river reaches. The impacts of sediment mining on the water level in the main channels were gradually negligible with the increasing flow discharge of each river section. In particular, in the Guangyangba channel, the sand excavation pit is approximately 100 m × 50 m, and the water levels upstream and downstream decrease during low flow discharge at a decline range of 0–0.07 m. Further, the maximum fluctuation occurred near the borrow pit, at approximately 0.07 m, and the decreasing trend approached zero when the distance increased to 1.2 km downstream (Fig. 20a). The river pattern of the Luoqi reach is relatively straight. It has sediment mining

that results in a very small water level decrease near its excavation pits, at a magnitude of approximately 0.025 m (Fig. 20b). Moreover, its influence propagation can extend to 1.5 km downstream. Conversely, the Changshou and Qinyanzi channels meander, creating more intense changes in their gravel extraction areas than in the Luoqi channel, decreasing by up to 0.047 m and 0.043 m, respectively (Fig. 20c, d). These results indicate that the sand excavation pits near the main channels can lead to a decrease in the navigable water level, and the influence density for navigation conditions can be determined by the sediment mining site and the magnitude of the flow discharge.

Conclusions

Herein, changes in the TGR navigation conditions were investigated, and the influencing factors of water-sediment discharge supply, sediment behavior, and sediment mining were analyzed. In 2008, after the operation of the TGD, minimum maintenance waterway depths in the PBA and FBA changed from 2.9 and 2.7 m to 4.5 and 2.9 m, respectively. In the PBA, a decline trend in the water-sediment supply may have further alleviated fine grained sedimentation, helping to maintain the navigable depth in the navigation- obstructing channels

Table 6 Initial and boundary parameters of numerical model

No.	Flow discharge (m³/s)	Outlet water level (m)	Sediment mining
SC-1	4500	146.53	No
SC2	4500	146.53	Yes
SC-3	9400	150.03	No
SC-4	9400	150.03	Yes
SC-5	14600	152.53	No
SC-6	14600	152.53	Yes
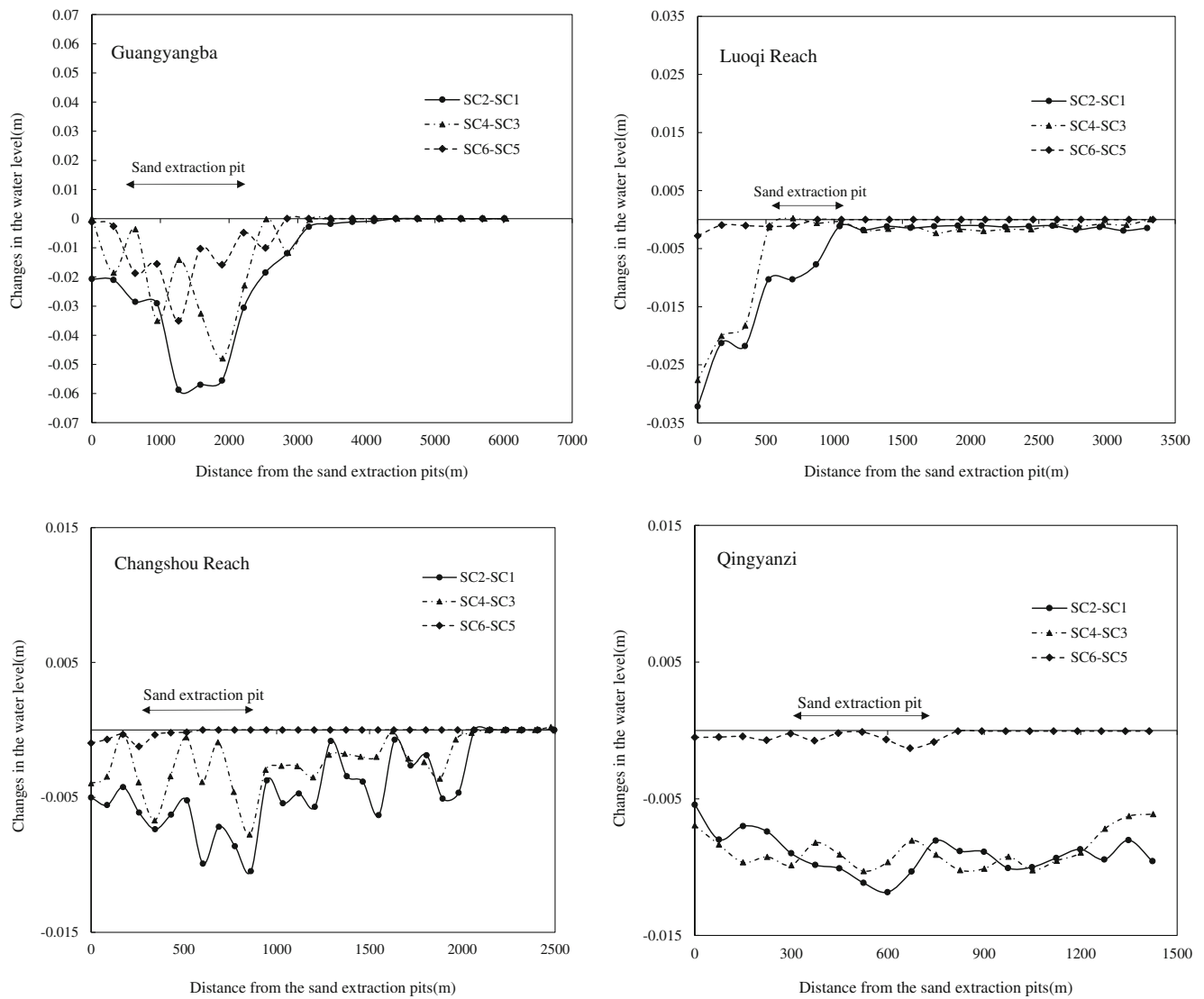
Fig. 20 Changes in the water level after sediment mining activity in the channels of (**a**) Guangyangba, (**b**) Luoqi, (**c**) Changshou, and (**d**) Qinyanzi

experiencing fine sedimentation. Conversely, in the FBA, bed load movement and temporary deposition led to a shortage of navigation depth clearance during the falling stage, especially in the Luoqi, Changshou, and Qingyanzi channels. Thus, during a high water-sediment discharge year, these channels should focus on maintaining the minimum waterway depth both in the falling stage and the subsequent falling stage. Moreover, sediment mining in the TGR decreased the navigable water level near the excavation pits, negatively impacting waterway depth during low flow discharge. Further, we found that sediment mining has an influence area that ranges from 1.0 to 1.5 km, as determined by the scale and site of the sediment excavation. These findings provide useful information for assessing navigation maintenance in the TGR. In addition, a 2D hydrological sediment numerical model was employed to predict channel patterns, wherein the correction terms for bed load transport of the secondary flow were empirical. The results of this model could be improved if a 3D model was applied to simulate the helical flow of the river bend. Further, additional research is necessary regarding the governing equation of alluvial river evolution in order to ensure the availability of the numerical models. Also, extreme hydrological years should be considered to investigate the change trends of navigation conditions in the subsequent next falling stage.

Declarations

Conflict of interest The authors declare no conflict of interest.

References

Cao F, Xiao X, Wu P (2010) Yangtze River: China's golden waterway. Civ Eng 163(5):15–18

Chen Z, Li J, Shen H, Zhang HW (2001) Yangtze River of China: historical analysis of discharge variability and sediment flux. Geomorphology 41:77–91

Cheng JX, Xu L, Wang XL (2018) Assessment of hydrologic alteration induced by the Three Gorges Dam in Dongting Lake, China. River Res Appl 1:1–11

CWRC (2017) Bulletin of Changjiang Sediment. Changjiang Press, Wuhan, China

CWRC (2019) Bulletin of Changjiang Sediment. Changjiang Press, Wuhan, China

Dai ZJ, Liu JT (2013) Impacts of large dams on downstream fluvial sedimentation: a example of the Three Gorges Dam (TGD) on the Changjiang (Yangtze River). J Hydrol 480:10–18

Dai SB, Lu XX (2014) Sediment load change in the Yangtze River (Changjiang): a review. Geomorphology 215:60–73

Huang Q, Sun ZD, Opp C, Lotz T (2014) Hydrological drought at Dongting Lake: its detection, characterization, and challenges associated with Three Gorges Dam in Central Yangtze, China. Water Resour Manag 28:5377–5388

Huang YN, Li YP, Ji DB (2016) Study on nutrient limitation of phytoplankton growth in Xiangxi Bay of the Three Gorges Reservoir, China. Sci Total Environ 723:232–258

International Research and Training Center on Erosion and Sedimentation (IRTCES) (2019) River sediment bulletin of china 2018. Beijing, Chinese

Jia DD, Shao XJ, Zhang XN (2013) Sedimentation patterns of fine-grained particles in the dam area of the Three Gorges Project: 3D Numerical Simulation. J Hydraul Eng 139:669–674

Li YT, Sun Y, Liu J (2009) Channel degradation downstream from the three gorges project and its impacts on flood level. J Hydraul Eng 135(9):718–728

Li SZ, Yang YP, Zhang MJ (2018a) Coarse and fine sediment transportation patterns and causes downstream of the Three Gorges Dam. Front Earth Sci 12:750–764

Li WJ, Yang SF, Xiao Y (2018b) Rate and distribution of sedimentation in the Three Gorges Reservoir, Upper Yangtze River. J Hydraul Eng 144:8

Lu Y, Zuo L, Ji R, Liu H (2010) Deposition and erosion in the fluctuating backwater reach of the Three Gorges Project after upstream reservoir adjustment. International Journal of Sediment Research 25:64–80

Mei X, Dai ZJ, van Gelder PH (2015) Linking Three Gorges Dam and downstream hydrological regimes along the Yangtze River, China. Earth Space Sci 2:94–106

Milliman JD, Meade RH (1983) World-wide delivery of river sediment to the oceans. J Geol 91:1–21

Munoz SE, Giosan L, Therrell MD (2018) Climatic control of Mississippi River flood hazard amplified by river engineering. Nature 556:95–98

Ren JQ, Zhao MD, Zhang W (2020) Impact of the construction of cascade reservoirs on suspended sediment peak transport variation during flood events in the Three Gorges Reservoir. Catena 188:115–126

Sediment-Panel (2018) Study on sediment problems in the Three Gorges Project on the Yangtze River (in Chinese). Construction committee for the Three Gorges Project. State Council of China, Beijing, China

Song K, Wang FW, Yi QL (2018) Landslide deformation behavior influenced by water level fluctuations of the Three Gorges Reservoir (China). Eng Geol 247:58–68

Sun ZD, Huang Q, Opp C, Henning T, Marold U (2012) Impacts and implications of major changes caused by the Three Gorges Dam in the middle reaches of the Yangtze River, China. Water Resour Manag 26:3367–3378

Wang ZY, Li Y, He Y (2007) Sediment budget of the Yangtze River. Water Resour Res 43:W04401

Wang S, Fu B, Piao S, Lü Y, Ciais P, Feng X, Wang Y (2016) Reduced sediment transport in the Yellow River due to anthropogenic changes. Nat Geosci 9(1):38–41

Wolf A, Bergmann A, Wilken RD, Gao X (2013) Occurrence and distribution of organic trace substances in waters from the Three Gorges Reservoir, China. *Environ Sci Pollut Res* 20:7124–7139

Xiao (2013) Control factors and threshold for transformation of fluvial channel patterns. Tsinghua University, Beijing, China

Xiao Y, Wang H, Shao IXJ (2014) 2D numerical modeling of grain-sorting processes and grain size distribution. J Hydro-environ Res 8:452–458

Xiao Y, Yang FS, Li JW (2015) Fluvial sedimentation of the permanent backwater zone in the Three Gorges Reservoir, China. Lake and Reservoir Management 31:324–338

Xiao Y, Zhou G, Yang SF (2016) 2D numerical modelling of meandering channel formation. J Earth Syst Sci 2(125):251–267

Xiao Y, Li WJ, Yang SF (2019a) Changing temporal and spatial patterns of fluvial sedimentation in Three Gorges Reservoir, Yangtze River, China. Arab J Geosci 12:490

Xiao Y, Yang SF, Wang T (2019b) Analysis on navigation condition of the Three Gorges Reservoir at initial stage of water storage. Port Waterway Eng (in Chinese) 11:96–101

Xiong M, Xu QX, Yuan J (2009) Analysis of multi-factors affecting sediment load in the Three Gorges Reservoir. Quat Int 208:76–84

Xu KH, Milliman JD (2009) Seasonal variations of sediment discharge from the Yangtze River before and after impoundment of the Three Gorges Dam. Geomorphology 104:276–283

Yan QY, Yu YH, Feng WS (2008) Plankton community composition in the Three Gorges Reservoir Region revealed by PCR-DGGE and its relationships with environmental factors. Journal of Environmental Sciences-China 20:732–738

Yan T, Yang YP, Li YB (2019) Possibilities and challenges of expanding dimensions of waterway downstream of Three Gorges Dam. Water Sci Eng 12:136–144

Yang ZJ, Liu DF, Ji DB, Xiao SB (2010) Influence of the impounding process of the Three Gorges Reservoir up to water level 172.5 m on water eutrophication in the Xiangxi Bay. Science China-Technological Sciences 53:1114–1125

Yang YP, Zhang MJ, Liu WL (2019) Relationship between waterway depth and low-flow water levels in reaches below the Three Gorges Dam. Journal of Waterway, Port, Coastal, and Ocean Engineering 145(1):04018032

Yuan YJ, Zeng GM, Liang J, Huang L, Hua SS, Li F et al (2015) Variation of water level in Dongting Lake over a 50-year period: implications for the impacts of anthropogenic and climatic factors. J Hydrol 525:450–456

Yue S, Pilon P, Phinney B, Cavadias G (2002) The influence of autocorrelation on the ability to detect trend in hydrological series. Hydrol Process 16:1807–1829

Zhang S, Jing Z, Li W, Wang L, Liu D, Wang T (2019) Navigation risk assessment method based on flow conditions: a case study of the river reach between the Three Gorges Dam and the Gezhouba Dam. Ocean Eng 175:71–79

Zheng S (2016) Reflections on the Three Gorges Project since its operation. Engineering 2(4):389–397

Zhou M, Xia J, Lu J, Deng S, Lin F (2017) Morphological adjustments in a meandering reach of the middle Yangtze River caused by severe human activities. Geomorphology 285:325–332